Biointerface Research in Applied Chemistry
Open-Access Journal (ISSN: 2069-5837)

Article
Volume 13, Issue 6, 2023, 521
https://doi.org/10.33263/BRIAC136.521

Synthesis and Antioxidant Activity of some novel 4*H*-Chromene Derivatives Catalysed by Biogenic Tin Oxide Nanoparticles

Mahesh Siddappareddy Gari [1], Boya Palajonnala Narasaiah [2], Anitha Pandurengan [3], Badal Kumar Mandal [4,*], Muruganantham Natarajan [1,*]

[1] PG&Research Department of Chemistry, Thanthai Hans RoeverCollege (Autonomous), (Affiliated to Bharathidasan University), Perambalur-621220, Tamilnadu, India; maheshreddysm@gmail.com (M.S); nmuruganphd@gmail.com (M.N.);
[2] Department of Physics, Indian Institute of Technology (IIT) Tirupati, Andhra Pradesh-517506, India; narsipalajonna@gmail.com (B.P.N.);
[3] Department of Physics, Roever Engineering College (Affiliated to Anna University)Elambalur, Perambalur, Tamilnadu, India; anithaphysics84@gmail.com (A.P.);
[4] Department of Chemistry, School of Advanced Sciences, Vellore Institute of Technology, Vellore - 632014, Tamil Nadu, India; badalkmandal@gmail.com (B.K.M.);
* Correspondence: nmuruganphd@gmail.com (M.N.); badalkmandal@gmail.com (B.K.M.);

Scopus Author ID 7102080708
Received: 23.09.2022; Accepted: 30.10.2022; Published: 4.02.2023

Abstract: The present study reports an eco-friendly and biogenic synthesis of Tin Oxide Nanoparticles (SnO_2 NPs) using aqueous sunflower leaf extract. The synthesized SnO_2 NPs were characterized using advanced analytical techniques such as X-day diffraction spectroscopy, UV-Visible spectroscopy, FT-IR spectroscopy, and Electron Microscopy. After observing the formation of SnO_2 NPs by UV-Vis spectroscopy, the crystalline nature of SnO_2 NPs was confirmed by powder XRD analysis. Fourier Transform Infrared Spectroscopy (FT-IR) analysis was used to check the attached functional groups on the surface of SnO_2 NPs due to the capping of phytochemicals during the reduction and stabilization of NPs by the plant's secondary metabolites. Size, crystallinity, and morphology were measured by High-resolution transmission electron microscopy (HR-TEM) analysis. The prepared SnO_2 NPs were used as a catalyst for synthesizing the novel 4*H*-chromene compounds via a multicomponent reaction of salisaldehydes, acetylacetone, and 4-Hydroxy coumarin by microwave method. All the compounds were characterized by ^1H and ^{13}C NMR spectroscopy. All the compounds and SnO_2 NPs were further screened for antioxidant activity using DPPH radical assay. All compounds showed a good percentage of inhibition with respect to standard ascorbic acid.

Keywords: sunflower leaves; SnO_2 NPs; phytochemicals; DPPH assay; 4H-chromenes; antioxidant activity.

1. Introduction

Researchers have paid more attention to the synthesis of small-size nanoparticles in the past decades to advance numerous technical applications in various fields. Among various metal oxide nanoparticles that have been performed in the last few decades, tin oxide nanoparticles (SnO_2 NPs) are one of the well-studied semiconducting NPs known for their enormous applications in biology, environmental monitoring, energy storage, supercapacitor,

etc. [1-5]. By taking advantage of these properties, synthesis methods of nanomaterials mainly focus on modifying the surface area of the nanoparticles through natural reducing and capping agents, which remains still challenging. Nevertheless, nanoparticles generated by green chemical agents such as plant extract must possess high stability and smaller size [6,7]. Moreover, green synthesized nanomaterials have been used in different research fields, such as environmental sciences, synthetic chemistry, nanotechnology, and material chemistry [8]. Earlier reports show that the nanoparticles have a significant effect on the application of photocatalytic activity [9], electrochemical sensors [10], anti-corrosion properties [11], and antituberculosis activity [12]. However, among various nanomaterials, SnO2 NPs are considered an alternative source for catalytically active materials for organic transformation [13,14].

Chromene and its analogs are important heterocyclic compounds generally found in natural products and biologically active compounds. The chromene compounds have excellent pharmacological and biological applications like anti-inflammatory [15], potential succinate dehydrogenase inhibitors [16], anti-gastric cancer activity [17], antimicrobial and antiproliferative activity [18], antibacterial [19], tyrosinase inhibitory [20], anticancer [21], antituberculosis [22], antidiabetic [23], anticholinesterase [24], antioxidant [25], antiepileptic [26], anti-HIV activity [27], and raw materials in making of dyes and pigments [28]. Due to the high potential activity of 4*H*-chromenes, several methods have been employed for their synthesis. Chitreddy and Shanmugam reported the synthesis of 4*H*-chromene derivatives by using CAN catalyst via multicomponent reaction of 2-hydroxy benzaldehydes, acetoacetanilides, and 4-hydroxy coumarins under solvent-free conditions [29]. Yu and co-workers reported Ni(II) complex and p-toluene sulfonic acid (PTSA) catalyzed one-pot synthesis of 4H chromenes from ortho-quinone methide and di-carbonyls [30]. Gaikwad and Kamble reported the synthesis of 4*H*-chromenes under microwave conditions in an aqueous hydrotropic medium via a three-component reaction of aromatic aldehydes, malononitrile, with 1- naphthol and 2-naphthol [31]. Li and his group reported the synthesis of 4*H*-chromenes via a three-component reaction of ketoesters with naphthols by using bismuth trifluoromethane sulfonate [$Bi(OTf)_3$] [32]. Although the published reports are efficient for the functionalized 4*H*-chromenes via three-component reactions, they are facing some harsh conditions like difficult workup procedures, reaction time, reaction yield, and expensive solvents and catalysts. In continuation to our efforts to synthesize biologically important 4*H*-chromenes we developed a new synthetic pathway in solvent-free conditions byKnoevenagel-Michael reaction of salisaldehydes, acetylacetone with 4-hydroxycoumarin under microwave conditions in good to excellent yields.

2. Materials and Methods

2.1. Materials and methods.

Tin(II) chloride dihydrate ($SnCl_2.2H_2O$) salt was purchased from Sigma-Aldrich, India. The sunflower leaves were collected from the Tungabadra river area, Elamandyam village, Andhra Pradesh, India. All analytical grade chemicals were used. Distilled water was used as a solvent throughout this study. The completion of the reaction was monitored using TLC. The λ_{max} values were calculated by UV-Visible spectrophotometer (Shimadzu, model-UV-1601), and FT-IR spectrophotometer (Shimadzu model- IR-Affinity) was used for characterization of

functional groups attached to SnO_2 NPs' surfaces. The Bruker-400 MHz NMR was used for recording Chemical shift values in $CDCl_3$ solvent.

2.2. Preparation of the leaf extract.

Sunflower leaves were collected from the Tungabadra river area, washed with running tap water, followed by distilled water to remove the unwanted waste and dust particles, and dried at room temperature for 7 days. Then the dried leaves were ground by an eclectic mixer and sieved through 100 mesh sieve standards. The extract was prepared after mixing 3 g of dried sunflower leaves fine powder in 100 mL of distilled water on a hot plate for 60 min at 80 °C. The extract was filtered using Whatman No.1 filter paper and stored at 4 °C for further use.

2.3. Green synthesis of SnO_2 nanomaterials from sunflower leaf extract.

To prepare tin oxide nanoparticles, 0.564 g of tin chloride (0.05M) was dissolved in 50 mL of distilled water and then followed by the addition of 50 mL of aqueous sunflower flower leaves extracts and mixed simultaneously, stirred thoroughly at 80 °C, 3 h reflux condition and after 30 min, the change of color was observed to light yellow from milky white. Finally, the collected colloidal mixture was centrifuged for 30 min at 6000 rpm. To reduce the impurities and large biomolecules, the yellow precipitate was washed thoroughly with ethanol solvent, followed by distilled water. Once again, the centrifuged process was repeated with the same condition till the fine pellet was obtained and then transferred to a 50mL beaker, followed by heating on a hotplate at 60 °C temperature. The resultant precursor was crushed into powder form, followed by annealing at 500 °C for 3h. Consequently, the fine powder of SnO_2 NPs was collected and stored for further use.

2.4. Characterisation of the tin oxide nanomaterials.

UV-Visible spectroscopy was used for the characterization of SnO_2NPs' optical properties. The Ultrasonic bath (make-Enertech) was used for SnO_2NPs' dispersion in water, and the dispersion was used for absorbance measurement. The band gap energy of NPs was detected by UV-Vis-NIR spectrophotometer (make-JASCO v-670). The functional groups of sunflower leaf extract and biogenic SnO_2NPs were detected by FTIR spectroscopy (make-Shimadzu) using KBr pellets. The X-ray diffraction analysis was carried out after coating SnO_2 nanoparticles onto the XRD grid and recording Bragg's reflections in the ranges of 10-90° with a 4°/min scanning rate. The size and morphology of SnO_2NPs were characterized by HR-TEM (make-JEOL, JEM 2100 USA) using a Cu grid with a resolution of 0.1nm and voltage of 200 kev.

2.5. DPPH radical scavenging activity of SnO_2 NPs and 4H-chromene compounds.

The DPPH scavenging activity was conducted per the reported method with minor modifications. In brief, 1 mL of 0.1mM DPPH solution was added to 3 mL of the synthesized SnO_2NPs' dispersion, and 4H-chromene derivatives (4a-e) were added at different concentrations, such as 1, 2, 3, and 4 µM. The samples were incubated for 30min in dark conditions. Afterward, the test and control samples were recorded at 517 nm by using a UV-Visible spectrophotometer. Ascorbic acid was used as standard. The % of inhibition and IC_{50} values were measured by the following formula.

$$\% \text{ of inhibition} = [A_c\text{-}A_t/A_c] \times 100$$

where, A_c is the absorbance for the control sample, A_t is the absorbance of the test sample.

2.6. General method for synthesis of 4H-chromenes (4a-e).

The three-component mixture of 2-hydroxybenzaldehydes 1(a-b) (1 mmol), acetylacetone2(a-b) (1mmol), 4-hydroxycoumarin 3 (1mmol), and 25mole % of SnO2 NPs was taken into 100 mL round bottom flask under neat condition and was exposed to microwave irradiation at 200W for 4 min. Then the mixture was cooled to room temperature, followed by crushed ice to get the solid product infiltration.

3. Results and Discussion

3.1. UV-visible analysis.

The optical properties of SnO_2 NPs and their band gap energy were calculated by UV-Visible spectroscopy, which is represented in Figure 1. The strong absorption band at about 256.42 nm confirms the formation of SnO_2NPs (Figure 1A). A similar result was reported for the synthesis of SnO_2Quantum dots using ParkiaSpeciosaHassk Pods aqueous extract; however, they noticed an absorption band shoulder peak at 270 nm [33]. UV-Vis diffuse reflectance mode (UV-Vis-DRS) study was carried out to determine the band gap energy of SnO_2NPswitha wavelength range of 200-800 nm. The band gap energy was calculated by using the following formula as $(\alpha h\upsilon)^2 = A(h\upsilon\text{-}Eg)^n$, where α is the absorption coefficient, A is the constant, hυ is the photon energy, and n=2 for direct transition and Eg is the band gap energy. Figure 1(B) shows the graphical plot of hυ vs. $(\alpha h\upsilon)^2$ by using origin 8.5 software, and the Tauc plot gives the optical band gap energy of 3.37 eV.

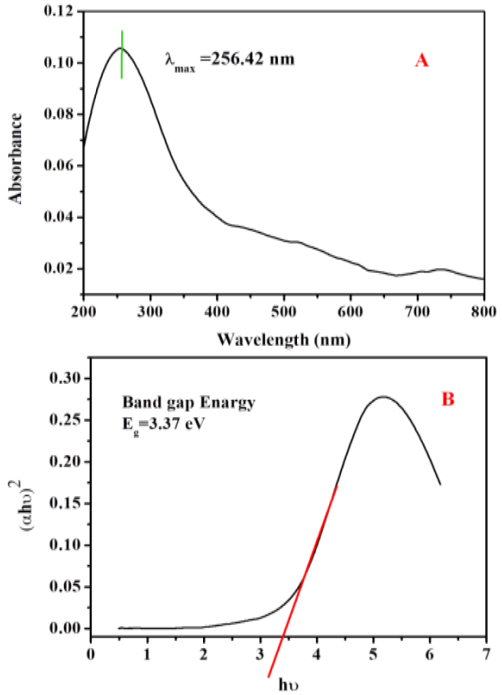

Figure 1. Optical properties of SnO_2NPs by UV-Visible spectroscopy: **(A)** absorption band and **(B)** band gap energy of SnO_2NPs.

3.2. XRD analysis.

X-ray diffraction (XRD) analysis was carried out to investigate the crystalline nature of the SnO_2NPs as well as their phase purity. Figure 2A describes the XRD pattern of SnO_2NPs.

The diffractogram shows the appearance of nine characteristic diffraction peaks at *hkl* values of 110, 101, 200, 211, 220, 310, 112, 202, and 321, corresponding to the reflection at 2θ values of 26.57°, 33.63°, 37.93°, 51.75°, 54.64°, 61.91°, 64.99°, 71.39°, and 78.67° respectively. The lattice plane with *hkl*(110) value is more intense, indicating the formation of a small crystallite size of SnO_2NPs (JCPDS N0: 96-152-6638).

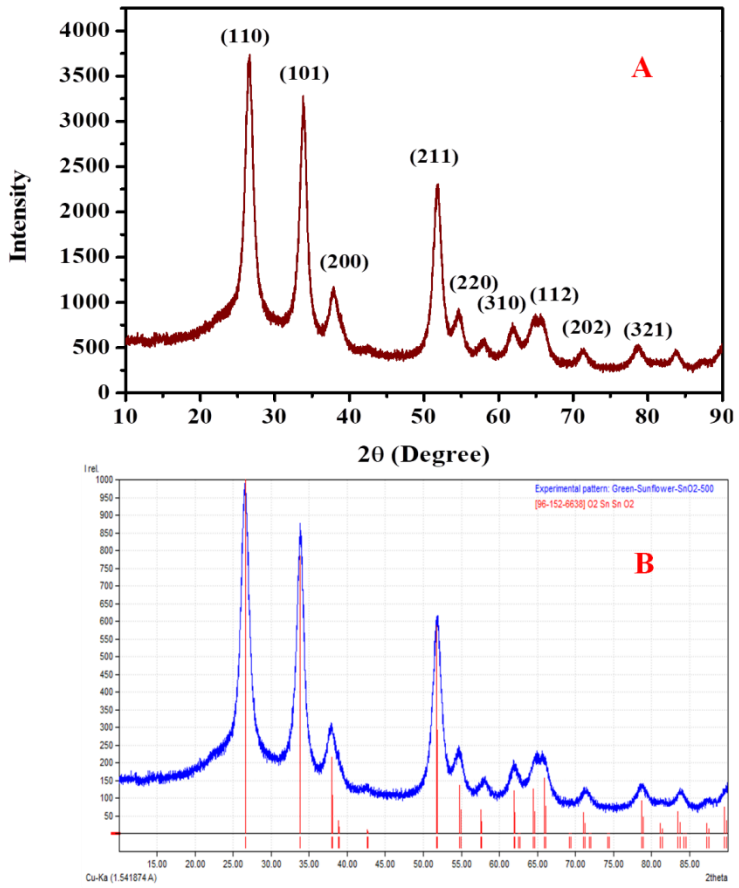

Figure 2. (A) XRD pattern of SnO_2 NPs annealing at 500°C and **(B)** XRD diffraction pattern match with the Match3 software (SnO_2NPs).

The XRD diffraction pattern of SnO2NPs matches with the Match3 software (Figure 2B). The obtained diffraction pattern corresponds to the tetragonal rutile structure of the synthesized SnO2NPs. The average crystallite size was calculated by Scherrer's equation as $D=k\lambda/\beta\cos(\theta)$, where D is the average crystallite size, K is the Scherrer's coefficient (0.891), λ is the X-ray wavelength (λ=1.5406 Å), β is the full width at half maximum intensity (FWHM) in radians, and θ is Bragg's angle. The calculated crystallite size of SnO_2 NPs was 12.34 nm. A similar type of SnO_2 NPs was synthesized using Piper betel leaves; however, the average crystalline size of the synthesized SnO_2NPs was 12 nm, which was determined by Scherrer's equation. Our result is in good agreement with them [34].

3.3. FT-IR analysis.

Figure 3 represents FT-IR spectra of sunflower leaf extract and SnO_2NPs recorded at 4000-500 cm^{-1}. The spectrum shows a strong absorbance peak at 3368.56 cm^{-1}, corresponding to the –OH stretching vibration of polyphenols capped on the NPs' surfaces during synthesis.

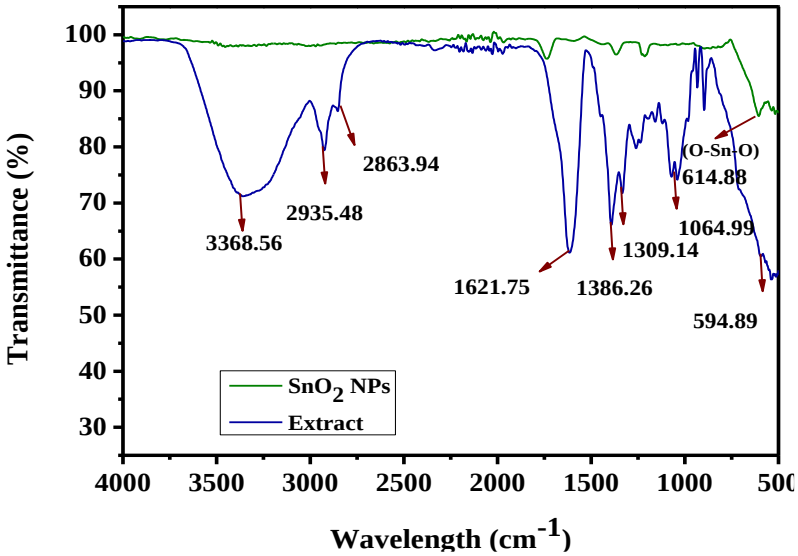

Figure 3. FT-IR spectra of SnO_2NPs and sunflower leaves aqueous extract.

The absorption band located at around 2935.48 cm^{-1} and 2863.94 cm^{-1} can be attributed to symmetric as well as asymmetric –CH stretching vibration of the methyl group, respectively. The strong absorption band at 1621.75 cm^{-1} for –N–H stretching vibration of the amine functional group, a strong band at 1386.26 cm^{-1} could be assigned to –C–O–C– stretching vibration of the ester functional group, a small band at 1309.14 cm^{-1} could be assigned to –C–N stretching vibration of ester functional group, while a weak absorption band at 1064.99 cm^{-1} is associated with the –C–O–H bending vibration and band at 594.89 cm^{-1} for –C–H bending vibration of alkane. Figure 3 shows the FTIR spectrum of SnO_2NPs. The new stretching vibration peak appeared at 437.84 cm^{-1}, corresponding to metal, oxygen, and metal (O–Sn–O) stretching vibration. No other peaks appeared, indicating the purity of the synthesized SnO_2NPs. Narasaiah *et al*. (2022) reported [35] the presence of various functional groups in agro-waste cotton boll peel aqueous extract, which was responsible for the synthesis of SnO_2 NPs, and all bands appeared within 4000-500 cm^{-1}, which indicated the presence of polyphenols such as phenolic acids, cellulose, terpenoids, flavonoids, alkaloids, and proteins compounds.

3.4. TEM analysis.

The morphology and size of the synthesized SnO_2NPs were confirmed by high-resolution transmission electron microscopy (HR-TEM). Figure 4 A-D describes the TEM images of SnO_2NPs at different magnifications, such as 10 nm, 20 nm, 50 nm, and 100 nm. Figure 4E shows a selective area electron diffraction (SAED)pattern, which gives clear information on the polycrystalline nature of SnO_2NPs. Figure 4A-C shows the particle distribution at various magnifications of SnO_2NPs, and it is observed that most of the NPs are spherical without any agglomeration with a size range between 3-9 nm. The average particle size is calculated as 6.58 nm. Figure 4D represents the d-spacing of SnO_2NPs, and its value is 0.325 nm, which is in good agreement with the XRD result.

Figure 4E shows a selective area electron diffraction (SAED) pattern, which gives clear information about the crystallinity nature of SnO_2NPs. From the obtained results size and lattice planes of SnO_2NPs are in good agreement with the XRD data results. An earlier similar result was reported by Chang *et al*. [36]. Figure 4F shows the elemental composition of SnO_2NPs obtained from the energy dispersive X-ray spectroscopy (EDAX) study, which

suggests that the atomic percentage and atomic weight percentage of tin and oxygen elements in NPs are tin (wt%21.79, Atamicwt%15.59) and oxygen (wt%10.60, atomic wt%56.27) respectively, while the remaining atomic peaks in SAED pattern are due to copper grid which confirms the purity of SnO_2NPs. From the above data, we can conclude that the SnO_2 NPs are pure and crystalline.

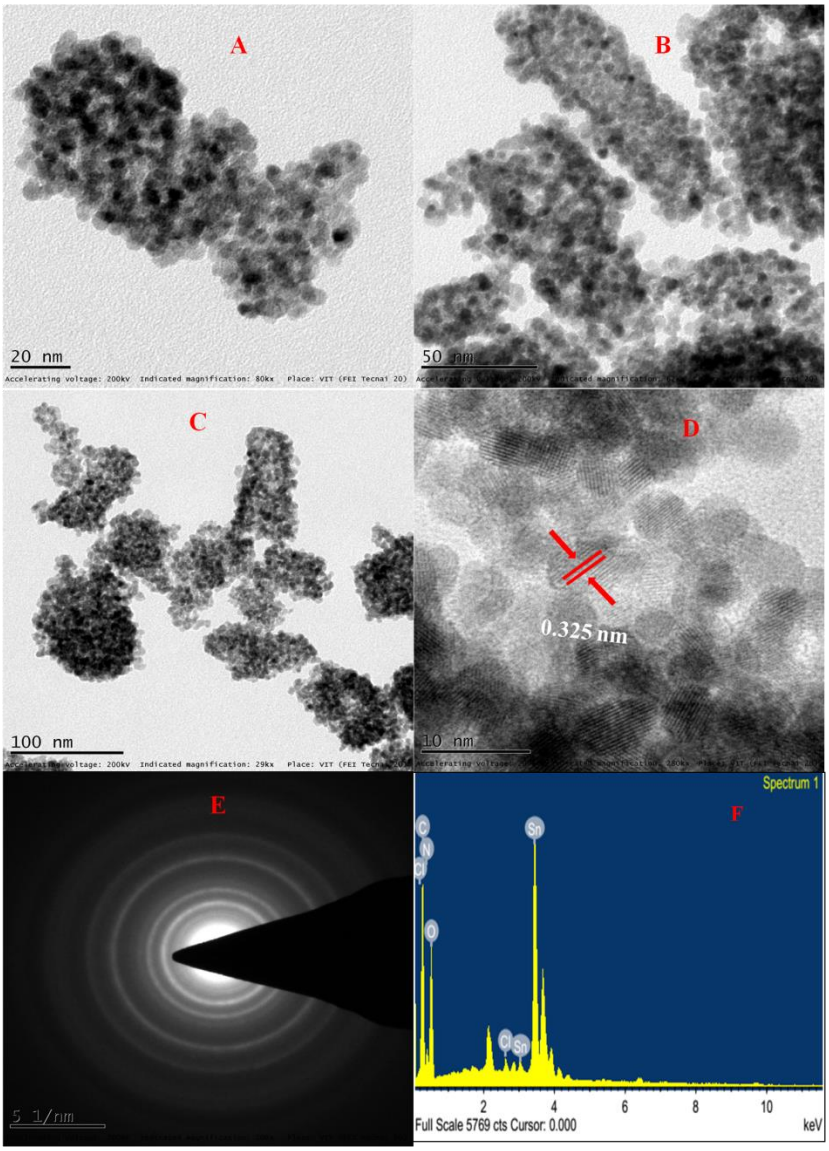

Figure 4. (A-C) TEM images of SnO_2NPs at different magnifications of 20 nm, 50 nm, and 100 nm**, (D)** inter planer distance (d-spacing value)**, (E)** SAED pattern**, (F**) elemental analysis of SnO_2NPs.

3.5. Synthesis of 4H-chromenes.

Initially, the multicomponent reaction was carried out to synthesize the 4*H*-chromene compound 4a (Figure 5); we took 2-hydroxybenzaldehyde 1a (1mmol), acetylacetone 2a (1mmol) and 4-hydroxycoumarin 3(1mmol) at 110°C for 8h in a round bottom flask under solvent and catalyst-free conditions and there was no progress of the reaction (Table 1, entry 1). Later the reaction was performed without a catalyst with DMF as a solvent, and the product was not formed(Table 1, entry 2). Using base catalyst piperidine at 100°C under the neat condition, we observed an increased yield of product 4a (Table 1, entry 3). Based on the piperidine base's experimental results, we used different base catalysts, such as triethylamine and pyrrolidine, which afforded the desired 4H-chromene product 4a in 41% and 33% of yield,

respectively (Table 1, entry4-5). The 39% of the product yield was achieved by using strong base NaOH at 100°C for 10h (Table 1, entry 6). However, with PTSA, we observed increased product yield(Table 1, entry 7). When we carried out the reactions in the presence of organic catalysts, i.e., DMAP, DABCO, and CAN, at 100°C for 6h, the obtained product 4*H*-chromene were 51, 53, and 61%, respectively (Table 1, entry 8-10). When the reaction was tried with an L-proline catalyst for 3h at 80°C under neat conditions, product 4a was in 65% yield (Table 1, entry 11).

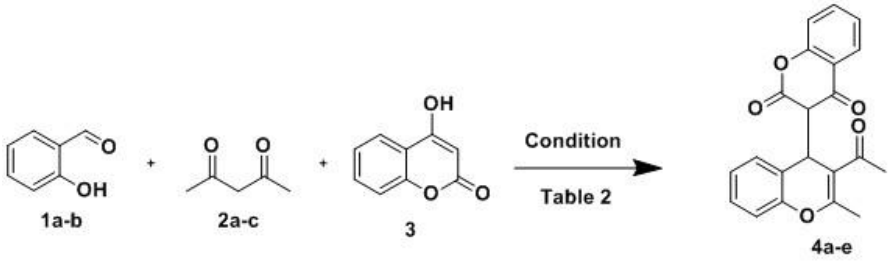

Figure 5. synthesis of 4*H*-chromenes.

After several reactions with different catalysts, the product yield of 4*H*-chromenes was moderate. It is observed that better product yields (70-73%) were obtained with SnO_2 NPs as a catalyst due to the increased electrophilicity at the carbonyl group of carbon represented in Figure 7. From the results, we could not find better yields using conventional methods. To improve the product yield, we tried the reaction with a non-conventional energy source, microwave irradiation. We started the reaction at 100w for 3 min (Table 1, entry 1) in the absence of the nanocatalyst with a trace of product 4a. The same reaction was carried out in the presence of the nanocatalysts, which provided the product with a 45% of yield (Table 1, entry 2).

Table 1. Optimizing the conventional method for synthesis of compound 4a[a].

Entry	Catalyst (25%)	Time (h)	Temperature (°C)	Yield (%)
1	--	8	110	NR
2	DMF	10	100	NR
3	Piperidine	10	100	14
4	Pyrrolidine	8	100	33
5	Triethylamine	10	100	41
6	NaOH	10	100	39
7	PTSA	5	100	57
8	DMAP	6	100	51
9	DABCO	6	100	53
10	CAN	6	100	61
11	L-Proline	3	80	65
12	SnO_2 NPs	2	100	70
13	SnO_2 NPs	2	120	73
14	SnO_2 NPs	3	120	73

[a]All the reactions were carried out in 1:1:1 ratio of substrates 1, 2, and 3 under neat conditions.

To stabilize the reaction condition for the synthesis of 4*H*-chromenes, reaction parameters such as microwave irradiation power, the mole ratio of the substrates, and time were considered. Thus, a reaction of the same mole ratio of compounds with 100w for 5 min in microwave power yielded a product of 45% (Table 2, entry 3). Later we increased the power to 150w for 2 min; the yield of the product(52%) was increased significantly(Table 2, entry 4). 61% of the product yield was recorded at a constant power of 150 w for 4min (Table 2, entry 5). The reaction yield with 200w for 4 min was increased to 90% (Table 2, entry 6). To optimize the conditions with a different mole ratio of substrates afforded 90% of desired product 4a

(Table 2, entries 7-8). It indicates that lower power decreased the product yield compared to reactions that were carried out at high microwave power. Increased microwave power and irradiation time caused the product yield 4a with no improvement or lower yield (Table 2, entries 9-10). Hence, conditions shown in entry 6 of Table 2 were found to be optimum for 4*H*-chromene derivatives, as shown in Figure 6.

Table 2. Optimizing the MW method for synthesis of 4H-chromene compound 4a [a,b].

Entry	Substrates ratio	MW power (watt)	Time (min)	Yield (%)[c]
1	1:1:1	--	3	Traces
2	1:1:1	100	3	45
3	1:1:1	100	5	45
4	1:1:1	150	2	52
5	1:1:1	150	4	61
6	1:1:1	200	4	90
7	1:2:1	200	4	90
8	2:1:1	200	4	90
9	1:1:1	300	4	88
10	1:1:1	300	6	84

[a]All reactions were conducted on CEM to discover 300 MW synthesizer without solvent [b]Mode 50psi at 100°C[c] Isolated product yield[d]Optimized condition.

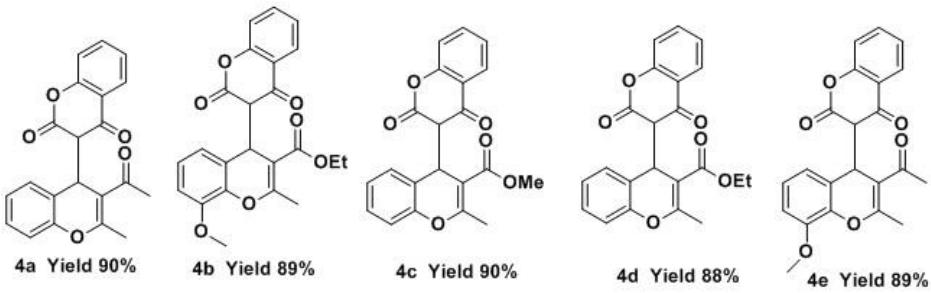

Figure 6. Diversity of synthesized 4*H*-chromene derivatives.

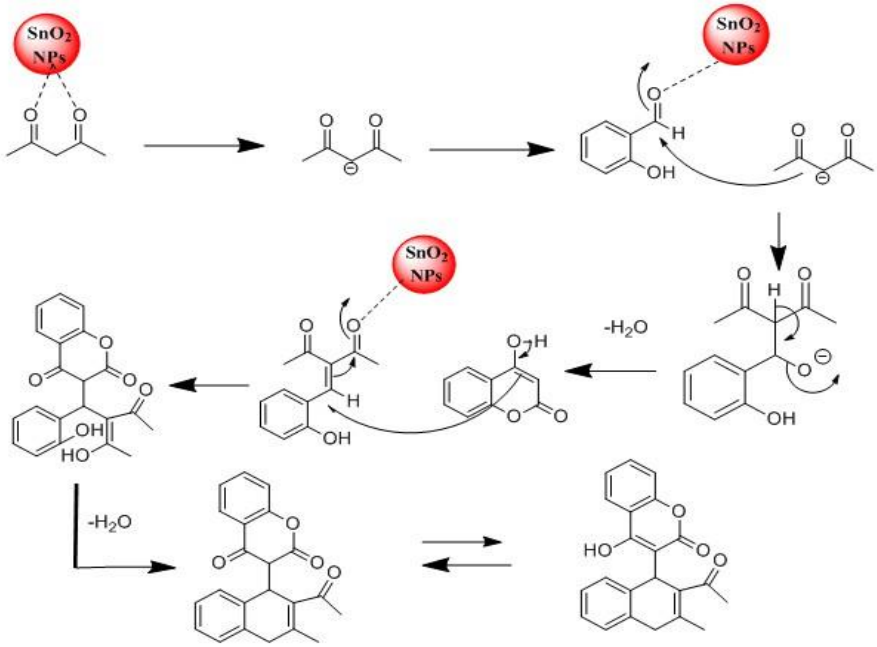

Figure 7. A plausible mechanism for the formation of 4*H*-chromenes.

3.6. Spectral data of the synthesized 4H-chromene derivatives (4a-e).

3-(3-acetyl-2-methyl-4H-chromen-4-yl)chromane-2,4-dione (4a)

Yellow solid; Mp: 148-150°C; ^{1}H NMR (400 MHz, $CDCl_3$): δ 7.89 (d, J = 7.6 Hz, 1H), 7.53-7.49 (m, 2H), 7.30-7.26 (m, 2H), 7.20-7.16 (t, 1H), 6.98-6.91 (m, 2H), 4.59 (d, J= 2.0 Hz, 1H), 3.38 (d, J=2.4Hz, 1H), 2.34 (s, 3H), 2.06 (s, 3H); ^{13}C NMR (100 MHz , $CDCl_3$) δ 202.57, 161.66, 158.82, 152.45, 150.43, 132.16, 128.69, 127.74, 125.11, 124.05, 123.09, 121.94, 116.60, 116.26, 114.62, 102.12, 99.11, 77.35, 77.04, 76.72, 49.61, 30.39, 29.93, 24.48.

Ethyl 4-(2,4-dioxochroman-3-yl)-8-methoxy-2-methyl-4H-chromene-3-carboxylate (4b)

Yellow solid; Mp: 140-142°C; ^{1}H NMR (400 MHz, $CDCl_3$): δ 7.86 (d, J= 6.8 Hz, 1H), 7.52-7.48 (t, 1H), 7.28-7.27 (m, 2H), 7.13 (d, J=6.8 Hz, 1H), 6.93-6.89 (t, 1H), 6.79 (d, J= 7.2Hz, 1H), 4.61 (s, 1H), 4.17-4.16 (q, 2H), 3.86 (s, 3H), 3.29 (s, 1H), 2.19(s, 3H), 1.25-1.22 (t, 3H); ^{13}C NMR (100 MHz , $CDCl_3$) δ 168.24, 161.52, 158.31, 152.46, 147.68, 139.86, 131.96, 126.09, 123.94, 123.07, 121.95, 119.70, 116.55, 114.65, 111.07, 103.18, 98.99, 61.52, 56.04, 43.74, 30.57, 24.92, 13.98.

Methyl 4-(2,4-dioxochroman-3-yl)-2-methyl-4H-chromene-3-carboxylate (4c)

White solid; Mp: 152-154°C; ^{1}H NMR (400 MHz, $CDCl_3$): δ 7.87 (d, J= 6.8 Hz, 1H),7.52 (d, J= 6.8Hz, 1H), 7.29-7.28 (m, 2H), 7.19-7.15 (t, 1H), 6.98-6.91 (m, 2H), 4.60 (s, 1H), 3.73 (s, 3H), 3.29 (s, 1H), 2.12 (s, 3H); ^{13}C NMR (100 MHz , $CDCl_3$) δ 168.74, 161.52, 158.12, 152.46, 150.56, 131.99, 128.56, 127.78, 125.02, 123.97, 122.96, 122.00, 116.61, 116.06, 114.70, 103.24, 98.94.

Ethyl 4-(2,4-dioxochroman-3-yl)-2-methyl-4H-chromene-3-carboxylate (4d)

Yellow solid; Mp: 144-146°C; ^{1}H NMR (400 MHz, $CDCl_3$): δ 7.87 (d, J= 8.0 Hz, 1H), 7.52-7.48 (m, 2H), 7.29-7.25 (m, 2H), 7.19-7.15 (t, 1H), 6.98-6.90 (m, 2H), 4.6 (s, 1H), 4.19-4.14 (q, 2H), 3.27 (s, 1H), 2.12 (s, 3H), 1.25-1.22 (t, 3H); ^{13}C NMR (100 MHz , $CDCl_3$) δ 168.27, 161.56, 158.17, 152.43, 150.53, 131.98, 128.55, 127.80, 125.03, 123.98, 122.95, 121.98, 116.60, 116.06, 114.68, 103.27, 99.00, 77.36, 77.04, 76.72, 61.53, 43.80, 30.63, 24.96, 14.00.

3-(3-acetyl-8-methoxy-2-methyl-4H-chromen-4-yl)chromane-2,4-dione (4e)

White solid; Mp: 147-149°C; ^{1}H NMR (400 MHz, $CDCl_3$): δ 7.87 (d, J= 8.0 Hz, 1H), 7.53-7.49 (t, 1H), 7.30-7.26 (m, 2H), 7.14 (d, J=8.0 Hz, 1H), 6.95-6.91 (t, 1H), 6.80 (d, J= 8.0 Hz, 1H), 4.6 (s, 1H), 3.87 (s, 3H), 3.40 (s, 1H), 2.34 (s, 3H), 2.13 (s, 3H); ^{13}C NMR (100 MHz , $CDCl_3$) δ 202.52, 161.63, 158.96, 152.47, 147.83, 139.76, 132.14, 126.14, 124.02, 123.21, 121.91, 119.61, 116.55, 114.58, 111.12, 102.03, 99.09, 56.05, 49.51, 30.32, 29.92, 24.44.

3.7. Antioxidant activity of SnO2 NPs and 4H-chromenes.

The DPPH radical scavenging activity of SnO_2 NPs and 4*H*-chromene derivatives (4a-e) was evaluated with DPPH assay. It is a good radical scavenger with an absorbance maximum of 517 nm in methanol. Its solution color is deep violet (λ_{max} 520 nm), but it becomes more stable and turns yellow after receiving hydrogen or electrons with lower absorbance. The IC_{50} values of the synthesized SnO_2 NPs and 4*H*-chromene compounds are demonstrated in Table 3. All the synthesized compounds show good antioxidant activity (Figure 8) when compared to standard antioxidant ascorbic acid.

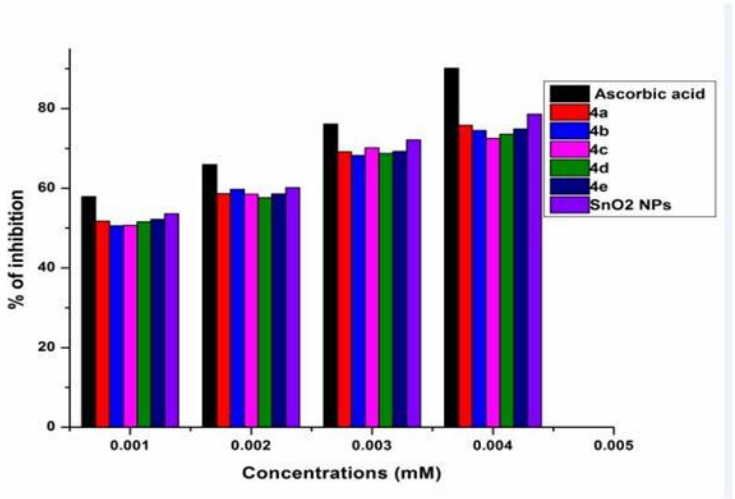

Figure 8. DPPH radical scavenging activity of SnO_2 NPs and the synthesized 4*H*-chromenes.

Table 3. IC_{50} values of 4*H*-chromene compounds.

Entry	Compound	% of inhibition at different concentrations (mM)				IC_{50}
		0.001	0.002	0.003	0.004	
1	4a	51.73	58.62	69.13	75.82	0.843
2	4b	50.61	59.72	68.23	74.52	0.857
3	4c	50.68	58.52	70.12	72.54	0.904
4	4d	51.58	57.63	68.75	73.54	0.865
5	4e	52.18	58.58	69.25	74.84	0.781
6	SnO_2 NPs	53.58	60.12	72.14	78.58	0.678
7	Ascorbic acid	57.92	65.93	76.12	90.12	0.424

4. Conclusion

Successfully synthesized SnO_2 NPs using an aqueous extract of sunflower leaves were characterized by XRD, and the crystal structure was tetragonal with an average crystallite size of 12.34 nm. In addition, the NPs were characterized by FTIR and UV-Vis spectroscopy. FT-IR analysis confirmed the capping of phytochemicals on the NPs' surface, while UV-Vis analysis calculated the optical band gap energy of 3.37 eV. HR-TEM images exhibited spherical shapes of SnO_2 NPs with an average size of 6.58 nm. A series of 4H-chromenes were synthesized by using SnO_2 NPs as nanocatalysts and were characterized by using ^{1}HNMR and ^{13}C NMR studies. The 4H-chromenes compounds were screened for antioxidant activity using a DPPH assay. All the compounds showed good antioxidant activity with respect to standard ascorbic acid and could be used in biomedical applications as well as antioxidants.

Funding

This research work has not received any external funding.

Acknowledgments

The authors are thankful to the management of Thanthai Hans Roever College and Vellore Institute of Technology for providing facilities to carry out this research work.

Conflicts of Interest

The authors declare no conflict of interest in this research work.

References

1. Yang, H.; Yu, G.; Liu, H. Synthesis of 3D flower-like SnO_2 with hierarchical nanostructureand high reversible capacity as lithium-ion battery anode. *J. Electron. Mater.* **2015**, *44*, 3744-3751, https://doi.org/10.1007/s11664-015-3840-3.
2. Jayachandiran, J.; Yesuraj, J.; Arivanandhan, M.; Muthuraaman, B.; Jayavel, R.;Nedumaran, D. Bifunctional investigation of ultra-small SnO_2 nanoparticle decorated rGO forozone sensing and supercapacitor applications. *RSC Adv.* **2021**, *11*, 856-866, https://doi.org/10.1039/D0RA10137K.
3. Narasaiah, B. P.; Mandal, B. K. Waste to wealth: a solution to textile dyes related pollution. *Mater.Res. Express* **2020**, *7*, 024001, https://doi.org/10.1088/2053-1591/ab6c22.
4. Sawabe, K.; Satsuma, A. Theoretical Study on Carbon Monoxide Adsorption onUnsupported and γ-Al_2O_3-Supported Silver Nanoparticles: Size, Shape, and Support Effects. *ACS omega* **2022**, *7*, 4405-4412, https://doi.org/10.1021/acsomega.1c06208.
5. Karmaoui, M.; Jorge, A. B.; McMillan, P. F.; Aliev, A. E.; Pullar, R. C.; Labrincha, J. A.; Tobaldi, D. M. One-step synthesis, structure, and band gap properties of SnO_2 nanoparticles made by a low temperature nonaqueous sol–gel technique. *ACS omega* **2018**, *3*, 13227-13238, https://doi.org/10.1021/acsomega.8b02122.
6. Narasaiah, B. P.; Banoth, P.; Dominguez, A. G. B.; Mandal, B. K.; Kumar, C. K.; Barnes,C. H.; Kollu, P. Biogenic Photo-Catalyst TiO_2 Nanoparticles for Remediation of Environment Pollutants. *ACS omega* **2022**, *7*, 26174–26189, https://doi.org/10.1021/acsomega.2c01763.
7. Matussin, S.; Harunsani, M. H.; Tan, A. L.; Khan, M. M. Plant-extract-mediated SnO_2nanoparticles: synthesis and applications. *Acs Sustain. Chem. Eng*. **2020**, *8*, 3040-054, https://doi.org/10.1021/acssuschemeng.9b06398.
8. Sinha, T.; Ahmaruzzaman, M.; Adhikari, P. P.; Bora, R. Green and environmentallysustainable fabrication of Ag-SnO_2 nanocomposite and its multifunctional efficacy as photocatalyst and antibacterial and antioxidant agent. *Acs Sustain. Chem. Eng*. **2017**, *5*, 4645-4655, https://doi.org/10.1021/acssuschemeng.6b03114.
9. Khan, R. ; Fulekar, M.H. Biosynthesis of titanium dioxide nanoparticles using Bacillus amyloliquefaciens culture and enhancement of its photocatalytic activity for the degradation of a sulfonated textile dye Reactive Red 31. *J. colloid interface sci* **2016**, *475*, 184-191, https://doi.org/10.1016/j.jcis.2016.05.001.
10. Zhu, C.; Yang, G.; Li, H.; Du, D.; Lin, Y. Electrochemical sensors and biosensors based on nanomaterials and nanostructures. *J.Anal.chem* **2015**, *87*, 230-249, https://doi.org/10.1021/ac5039863.
11. Zhang, S.; Liang, X.; Gadd, G.M.; Zhao, Q. Advanced titanium dioxide-polytetrafluorethylene (TiO_2- PTFE) nanocomposite coatings on stainless steel surfaces with antibacterial and anti-corrosion properties. *Appl.Surf.Sci* **2019**, *490*, 231-241, https://doi.org/10.1016/j.apsusc.2019.06.070.
12. Cui, J.; Wang, L.; Han, Y.; Liu, W.; Li, Z.; Guo, Z.; Hu, Y.; Chang, Z.; Yuan, Q.; Wang, J. ZnO nano-cages derived from ZIF-8 with enhanced anti mycobacterium-tuberculosis activities. *J.Alloys Compd* **2018**, *766*, 619-625, https://doi.org/10.1016/j.jallcom.2018.06.339.
13. Sarva, S.; Dunnutala, R.; Tellamekala, S.; Gundluru, M.; Cirandur, S. R. Green synthesisand antimicrobial activity of substituted diethyl (((5-(ethylthio)-1, 3, 4-thiadiazol-2-yl) amino)(phenyl) methyl) phosphonates. *Synth.Commun*. **2022**, *52*,1-12, https://doi.org/10.1080/00397911.2021.2020844.
14. Zolfigol, M.A.; Baghery, S.; Moosavi-Zare, A.R.; Vahdat, S.M.; Alinezhad, H.; Norouzi,M. Design of 1-methylimidazolium tricyanomethanide as the first nanostructured molten salt and its catalytic application in the condensation reaction of various aromatic aldehydes, amides and β-naphthol compared with tin dioxide nanoparticles. *RSC Adv.* **2015**, *5*, 45027–45037, https://doi.org/10.1039/C5RA02718G.
15. Chavan, P.; Pansare, D.; Shelke, R.; Shejul, S,; Bhoir, P. Ultrasound-assisted synthesis and biological significance of substituted 4H-chromene-3-carbonitrile using greeneryapproaches. *Curr. Chem. Lett*. **2021**, *10*, 43-52, http://dx.doi.org/10.5267/j.ccl.2020.7.003.
16. Lu, T.; Yan, Y.; Zhang, T.; Zhang, G.; Xiao, T.; Cheng, W.; Jiang, W.; Wang, J; Tang, X.Design, synthesis, biological evaluation, and molecular modeling of novel 4 H-chromeneanalogs as potential succinate dehydrogenase inhibitors. *J.Agric. Food Chem.* **2021**, *69*, 10709-10721, https://doi.org/10.1021/acs.jafc.1c03304.
17. Liu, J.; Wang, J.; Esmaeili, E.; Mollania, N.; Atharifar, H.; Keywanlu, M.; Tayebee, R.Biosynthesized CuO as a Green and Efficient Nanophotocatalyst in the Solvent-Free Synthesis of Some Chromeno [4, 3-b] Chromenes. Studying anti-Gastric Cancer Activity. *Polycycl. Aromat. Compd.* **2021**, 7071-7090, https://doi.org/10.1080/10406638.2021.1995012.

18. Abd-El-Aziz, A.S.; Alsaggaf, A.; Assirey, E.; Naqvi, A.; Okasha, R.M.; Afifi, T.H.; Hagar, M. A new family of benzo [h] chromene based azo dye: synthesis, in-silico and DFT studies with in vitro antimicrobial and antiproliferative assessment. *Int.J.Mol.Sci.* **2021**, *22*, 2807, https://doi.org/10.3390%2Fijms22062807.
19. Tajti, Á.; Szabó, K.E.; Popovics-Tóth, N.; Iskanderov, J.; Perdih, F.; Hackler, L.; Kari,B.; Puskás, L.G.; Bálint, E. PMDTA-catalyzed multicomponent synthesis and biological activity of 2-amino-4 H-chromenes containing aphosphonate or phosphine oxide moiety. *Org.Biomol.Chem*. **2021**, *19*, 6883-6891, https://doi.org/10.1039/D1OB01204E.
20. Karimian, S.; Ranjbar, S.; Dadfar, M.; Khoshneviszadeh, M.; Gholampour, M.;Sakhteman, A.; Khoshneviszadeh, M. 4H-benzochromene derivatives as novel tyrosinaseinhibitors and radical scavengers: synthesis, biological evaluation, and molecular docking analysis. *Mol.Divers.* **2021**, *25*, 2339-2349, https://link.springer.com/article/10.1007/s11030-020-10123-0.
21. Hafifi, T.; Mokasha, R.; Alsherif, H.; E.A Ahmed, H.; S Abd-El-Aziz, A. Design, synthesis, and docking studies of 4H-chromene and chromene based azochromophores: a novel series of potent antimicrobial and anticancer agents. *Curr.Org.Chem.* **2017**, *14*, 1036-1051, http://dx.doi.org/10.2174/1570179414666170519150520.
22. Zhao, W.; Wang, B.; Liu, Y.; Fu, L., Sheng, L.; Zhao, H.; Lu, Y.; Zhang, D. Design, synthesis, and biological evaluation of novel 4H-chromen-4-one derivatives asantituberculosis agents against multidrug-resistant tuberculosis. *Eur.J.Med.Chem.* **2020**, *189*, 112075, https://doi.org/10.1016/j.ejmech.2020.112075.
23. Soni, R.; Durgapal, S.D.; Soman, S.S.; Georrge, J.J. Design, synthesis and anti-diabeticactivity of chromen-2-one derivatives. *Arab.J.Chem*. **2019**, *12*, 701-708, https://doi.org/10.1016/j.arabjc.2016.11.011.
24. Tehrani, M.B.; Rezaei, Z.; Asadi, M.; Behnammanesh, H.; Nadri, H.; Afsharirad, F.; Moradi, A.; Larijani, B.; Mohammadi-Khanaposhtani, M.; Mahdavi, M. Design, Synthesis, and Cholinesterase Inhibition Assay of Coumarin-3-carboxamide-N-morpholine Hybrids as New Anti-Alzheimer Agents. *Chem.Biodivers.* **2019**, *16*, 1900144, https://doi.org/10.1002/cbdv.201900144.
25. Subbareddy, C.V.; Sundarrajan, S.; Mohanapriya, A.; Subashini, R.; Shanmugam, S.Synthesis, antioxidant, antibacterial, solvatochromism and molecular docking studies of indolyl-4H-chromene-phenylprop-2-en-1-one derivatives. *J.Mol.Liq.* **2018**, *251*, 296-307, https://doi.org/10.1016/J.MOLLIQ.2017.12.082.
26. Rawat, P.; Verma, S.M. Design and synthesis of chroman derivatives with dual anti-breast cancer and antiepileptic activities. *Drug Design, Development and Therapy* **2016**, *10*, 2779, https://doi.org/10.2147/DDDT.S111266.
27. Olomola, T.O.; Klein, R.; Mautsa, N.; Sayed, Y.; Kaye, P.T. Synthesis and evaluation of coumarin derivatives as potential dual-action HIV-1 protease and reverse transcriptase inhibitors. *Bio.Org.Medchem*. **2013**, *21*, 1964-1971, https://doi.org/10.1016/j.bmc.2013.01.025.
28. Azizi, N.; Mariami, M.; Edrisi, M. Greener construction of 4H-chromenes based dyes in deep eutectic solvent. *Dyes and Pigments* **2014**, *100*, 215-221, https://doi.org/10.1016/j.dyepig.2013.09.007.
29. Chitreddy, S.V.; Shanmugam, S. Solvent free-synthesis of highly functionalized 4H-chromene-3-carboxamide derivatives using cerium ammonium nitrate and their antioxidant, antibacterial and solvatochromism studies. *J.Mol.Liq.* **2017**, *243*, 494-502, https://dx.doi.org/10.1016/j.molliq.2017.08.058.
30. Yu, X.; Lan, W.; Li, J.; Bai, H.; Qin, Z.; Fu, B. Enantioselective one-pot synthesis of 4 H-chromene derivatives catalyzed by a chiral Ni (ii) complex. *RSC. Adv.* **2020**, *10*, 44437-44441, https://doi.org/10.1039/D0RA08906K.
31. Gaikwad, P.; Kamble, S. Microwave enhanced green and convenient synthesis of 2-amino-4H-chromenes in aqueous hydrotropic medium. *Current Research in Green and Sustainable Chemistry* **2020**, *3*, 100014, https://doi.org/10.1016/j.crgsc.2020.100014.
32. Li, H.J.; Luo, D.H.; Wu, Q.X.; Dai, C.Y.; Shen, Z.L.; Wu, Y.C. Bi (OTf) 3-catalyzedtandem reaction of naphthols with β, γ-unsaturated α-ketoesters. Efficient synthesis of functionalized 4H-chromenes. *Chin.Chem.Lett* **2014**, *25*, 1235-1239, https://doi.org/10.1016/j.cclet.2014.05.023.
33. Begum, S.; Ahmaruzzaman, M. Green Synthesis of SnO_2 quantum Dots Using ParkiaSpeciosaHassk Pods Extract for the Evaluation of Anti-Oxidant and PhotocatalyticProperties. *J.Photochem.Photobiol,B.* **2018**, *184* , 44–53, https://doi.org/10.1016/j.jphotobiol.2018.04.041.
34. Singh, J.; Kaur, N.; Kaur, P.; Kaur, S.; Kaur, J.; Kukkar, P.; Rawat, M. Piper betle leavesmediated synthesis of biogenic SnO_2 nanoparticles for photocatalytic degradation of reactiveyellow 186 dye under direct sunlight. *Environmental nanotechnology, monitoring &management* **2018**, *10*, 331-338, https://doi.org/10.1016/j.enmm.2018.07.001.

35. Narasaiah, B. P.; Banoth, P.; Sohan, A.; Mandal, B. K.; Bustamante Dominguez, A. G.;De Los Santos Valladares, L.; Kollu, P. Green Biosynthesis of Tin Oxide NanomaterialsMediated by Agro-Waste Cotton Boll Peel Extracts for the Remediation of Environmental Pollutant Dyes. *ACS omega* **2022**, *7*, 15423–15438, https://doi.org/10.1021/acsomega.1c07099.
36. Chang, J. H.; Cheong, J. Y.; Yuk, J. M.; Kim, C.; Kim, S. J.; Seo, H. K.; Lee, J. Y.Direct realization of complete conversion and agglomeration dynamics of SnO_2 nanoparticles in liquid electrolyte. *ACS Omega* **2017**, *2*, 6329-6336, https://doi.org/10.1021/acsomega.7b01046.